

Tunable Oxygen Diffusion and Electronic Conduction in SrTiO₃ by Dislocation-Induced Space Charge Fields

Kiran K. Adepalli, Jing Yang, Joachim Maier,* Harry L. Tuller,* and Bilge Yildiz*

Plastic strain engineering was applied to induce controllable changes in electronic and oxygen ion conductivity in oxides by orders of magnitude, without changing their nominal composition. By using SrTiO₃ as a model system of technological importance, and by combining electrical and chemical tracer diffusion experiments with computational modeling, it is revealed that dislocations alter the equilibrium concentration and distribution of electronic and ionic defects. The easier reducibility of the dislocation cores increases the n-type conductivity by 50 times at oxygen pressures below 10⁻⁵ atm at 650 °C. At higher oxygen pressures the p-type conductivity decreases by 50 times and the oxygen diffusion coefficient reduces by three orders of magnitude. The strongly altered electrical and oxygen diffusion properties in SrTiO₃ arise because of the existence of overlapping electrostatic fields around the positively charged dislocation cores. The findings and the approach are broadly important and have the potential for significantly impacting the functionalities of electrochemical and/or electronic applications such as thin film oxide electronics, memristive systems, sensors, micro-solid oxide fuel cells, and catalysts, whose functionalities rely on the concentration and distribution of charged point defects.

1. Introduction

The most common way to tune the electrical transport properties of oxides is by chemical doping. Recent advancements in making nanoscale thin films have provided alternative novel ways for going beyond bulk material properties, including hetero-interfaces.^[1–5] Generally in such interfacial systems, not only space charge effects^[2] but also elastic strain^[6–8] can serve as a control parameter to tune material properties. Thin film or hetero-interface structures made of yttria stabilized zirconia (YSZ)/SrTiO₃,^[3] CeO₂,^[9] SrZrO₃/RE₂O₃ (RE = rare earth),^[5] La_{1–x}Sr_xCoO_{3–δ}/SrTiO₃,^[10] (Nd,Sr)MnO₃/SrTiO₃,^[4]

Gd_{0.1}Ce_{0.9}O_{2–δ}/Er₂O₃,^[11] and Nd₂NiO₄/YSZ^[12] are examples of systems in which improved defect transport properties are attributed to thin film strain, albeit without distinction between the contributions of elastic strain versus dislocations. As initially proposed by Frank and van der Merwe,^[13] elastic strains resulting from larger lattice mismatch between epitaxial thin films and substrates are relieved plastically by formation of misfit dislocations. The film critical thickness (h_c) that leads to misfit dislocations, and the resulting dislocation density depends on misfit strain, elastic properties, and film thickness. According to the Matthews and Blakeslee^[14] model

$$h_c = \frac{b}{8\pi\epsilon} \frac{(1-\nu\cos^2\theta)}{(1+\nu)\cos\gamma} \left(\ln \frac{\alpha h_c}{b} \right) \quad (1)$$

where ϵ is lattice mismatch, ν is Poisson ratio, b is Burgers vector, θ is the angle between normal to slip plane and free surface, γ is the angle between Burgers vector and dislocation line, and α is core energy parameter, all corresponding to the thin film material. It is also possible to predict the spacing between misfit dislocations, d_{dis} , or equivalently the dislocation density $1/d_{\text{dis}}$, as^[15]

$$\frac{1}{d_{\text{dis}}} = \frac{2B\epsilon b_1(h-h_c)}{Bh^2b_1^2 + 2E_1'} \quad (2)$$

where B is the elastic constant given by $2G(1+\nu)/(1-\nu)$, G is the shear modulus, h is the film thickness, E_1' is the coefficient of expansion of the interaction energy and $b_1 = -b \sin\theta \sin\gamma$. Applicability of this theory has been demonstrated for a wide range of epitaxial thin film systems,^[15] and recent examples include oxide thin films made of La_{0.7}Sr_{0.3}MnO₃ grown on LaAlO₃.^[16] Equations (1) and (2) imply that it is possible to periodically arrange dislocations in thin films by exploiting the misfit strain, elastic properties, and film thickness between various combinations of film and substrate materials. While such features are widely explored in the semiconductor literature, forming and studying dislocations in functional oxide interfaces remain under-investigated. Recent interest along these lines in the oxide literature include YSZ thin films grown on Y₂O₃,^[17] on Gd doped CeO₂,^[18] or on MgO^[3,19] (in the order of increasing lattice strain) leading to misfit dislocations in YSZ at 12, 7, and 1 nm intervals, respectively. Given this ability to achieve a very high density of dislocations, with very small separation distance between them, it should be possible to tune

Dr. K. K. Adepalli, J. Yang, Prof. H. L. Tuller, Prof. B. Yildiz
Department of Materials Science and Engineering
Massachusetts Institute of Technology
Cambridge, MA 02139, USA
E-mail: tuller@mit.edu; byildiz@mit.edu

Dr. K. K. Adepalli, Prof. B. Yildiz
Department of Nuclear Science and Engineering
Massachusetts Institute of Technology
Cambridge, MA 02139, USA

Prof. J. Maier
Max Planck Institute for Solid State Research
Heisenbergstrasse 1, Stuttgart 70569, Germany
E-mail: s.weiglein@fkf.mpg.de

The ORCID identification number(s) for the author(s) of this article can be found under <http://dx.doi.org/10.1002/adfm.201700243>.

DOI: 10.1002/adfm.201700243

material properties via controlled plastic strain at oxide interfaces. Therefore, fundamental understanding of dislocations effect on the defect transport in oxides is important.

Dislocations are known to affect material properties and have been extensively investigated in metals^[20] and semiconductors^[21] over decades. However, the role that dislocations may play in impacting the chemical and physical properties of functional oxides has been under-investigated, in spite of their potential impact on the performance of these materials in important technologies, including solid oxide fuel cells,^[3,17,18] catalysts,^[22,23] resistive switching memory devices,^[24–29] and photoelectrochemistry.^[30,31] Our previous work^[32–34] has shown that the purposeful introduction of dislocations into TiO₂ was able to tune ionic and electronic conductivity via space charge effects (“1D doping”). In the last decade, several works^[25,26,35] indicated that resistive switching behavior in a prototypical oxide, SrTiO₃, is associated with dislocations, and some work also suggested that pipe diffusion of oxygen along dislocations assist resistive switching in this material.^[24] Theoretical studies,^[36,37] on the contrary, showed no possibility of pipe diffusion via dislocations in SrTiO₃. Recently, we predicted with the aid of atomistic simulations that $\langle 100 \rangle \{011\}$ edge dislocations in SrTiO₃ can accumulate high concentrations of positively charged oxygen vacancies in their core, while at the same time exhibiting lower oxygen vacancy mobilities compared to that in the bulk.^[36] The slower mobility found is consistent with the lack of pipe diffusion along another type of edge dislocation in SrTiO₃ reported experimentally and computationally.^[37,38] We also predicted that the space charge zone surrounding the dislocation should exhibit a lower concentration of oxygen vacancies due to electrostatic repulsion from the core,^[36] similar to the space charge regions near grain boundaries^[39] or surface^[40] of SrTiO₃. Such depression of the oxygen vacancy concentration would in turn suppress the oxygen diffusion coefficient within the space charge zones around the dislocations. There was no prior experimental proof for this predicted behavior in SrTiO₃. We return to these predictions when discussing the experimentally obtained correlations between dislocation density and ionic diffusivity and electronic conductivity in single crystalline SrTiO₃ in this paper.

To assess the net effect of dislocations on the defect chemistry, electronic conductivity, and oxide ion transport properties, both the core and the space charge zone around the dislocations must be considered. For this purpose, we took the nominally undoped (≈ 50 ppm Fe impurities) SrTiO₃ as a model oxide system. SrTiO₃ is a technologically important oxide, with relevance to a wide range of applications in the fields of oxide electronics,^[41,42] sensors,^[43] solid oxide fuel cell cathodes,^[44,45] solar cells,^[46,47] and memristive devices.^[27,48,49] The functionality of these electrochemical devices is highly dependent on the transport of electronic and ionic defects. Therefore, the bulk defect chemistry (of all charged species) of SrTiO₃ under equilibrium conditions has been extensively studied in the past;^[50–54] a summary of SrTiO₃ defect chemistry is provided in the Supporting Information. However, the applicability of bulk defect thermodynamics of the material becomes questionable for systems with a high density of dislocations. In the present work, we plastically deformed SrTiO₃ single crystals by an uniaxial hot press to create a high density of dislocations, and compared its properties with the reference SrTiO₃ single crystal.

2. Results

Figure 1a,b shows the two beam diffraction mode bright field transmission electron microscope (TEM) images of compressed crystals. Dislocations are observed on the $\{110\}$ plane when the electron beam axis is parallel to $[001]$. These findings agree with the slip systems^[55,56] in SrTiO₃ being the $\{110\}\langle 101 \rangle$. The plastically deformed samples had dislocation networks extending a few microns in length, and the distance between dislocations varied between 50–250 nm (Figure 1a,b). Based on several TEM images, we calculate the dislocation density to $\approx 10^9$ – 10^{10} cm⁻². It was difficult to obtain an accurate density measurement due to the inhomogeneous distribution of dislocations in the specimen. Dislocations remain unaltered even after an oxidation heat treatment at 1200 °C following the hot compression process. This indicates dislocations are stable and cannot be annihilated at moderate temperatures, especially in the temperature range of 500–700 °C where all the electrical and tracer diffusion characterizations were performed in this work. As described in the theory section (Section S1 of the Supporting Information), the electrical measurements as a function of oxygen partial pressure (pO_2) and temperature can be used to interpret the defect chemistry of an oxide.

Representative impedance spectra of the nominally undoped SrTiO₃ single crystals in their as-received state (from here on denoted as “pristine specimen or pristine SrTiO₃”) and after uniaxial hot compression (from here on denoted as “dislocations specimen or dislocations SrTiO₃”) are shown in Figure S1 in the Section S2 of the Supporting Information. Both specimens show a single arc with capacitance values on the order of that of the bulk crystal lattice (typically 10^{-11} F), we observed variation in the dielectric constant (Figure S2, Supporting Information). Figure 1c shows the pO_2 dependence of the electrical conductivity at 650 °C. The electrical conductivity data for the pristine SrTiO₃, agrees very well with the equilibrium bulk defect chemical and electrical conductivity data reported by others in the past.^[50,53,54,57] The slopes of conductivity versus pO_2 are $+1/4$ and $-1/4$ at high and low pO_2 , respectively, for the pristine specimen as known and expected from the bulk defect chemistry of undoped SrTiO₃ (see Section S1 in the Supporting Information). The dislocations specimen also shows a transition from $+1/4$ to $-1/4$ as the pO_2 is reduced, but importantly the extrapolated conductivity minimum shifted by seven orders of magnitude toward higher pO_2 compared to that of the pristine specimen. At high pO_2 , both specimens exhibit a $+1/4$ slope in conductivity versus pO_2 , typical characteristics of holes according to Equation S12 in the Supporting Information. However, the introduction of dislocations has led to an overall decrease in p-type conductivity by approximately two orders of magnitude. In contrast, at lower pO_2 , i.e., below 10^{-10} atm, the dislocations specimen also has a higher n-type conductivity by about two orders of magnitude, and with a $-1/4$ slope in conductivity versus pO_2 , typical characteristics of electrons according to Equation S8 in the Supporting Information. At even lower pO_2 ($< 10^{-15}$ atm), a transition to a $-1/6$ slope, characteristic of intrinsic electronic compensation (according to Equations S3–S5 in the Supporting Information) takes place only for the dislocations specimen. The fact that the conductivity minimum shifted by about seven orders of magnitude to

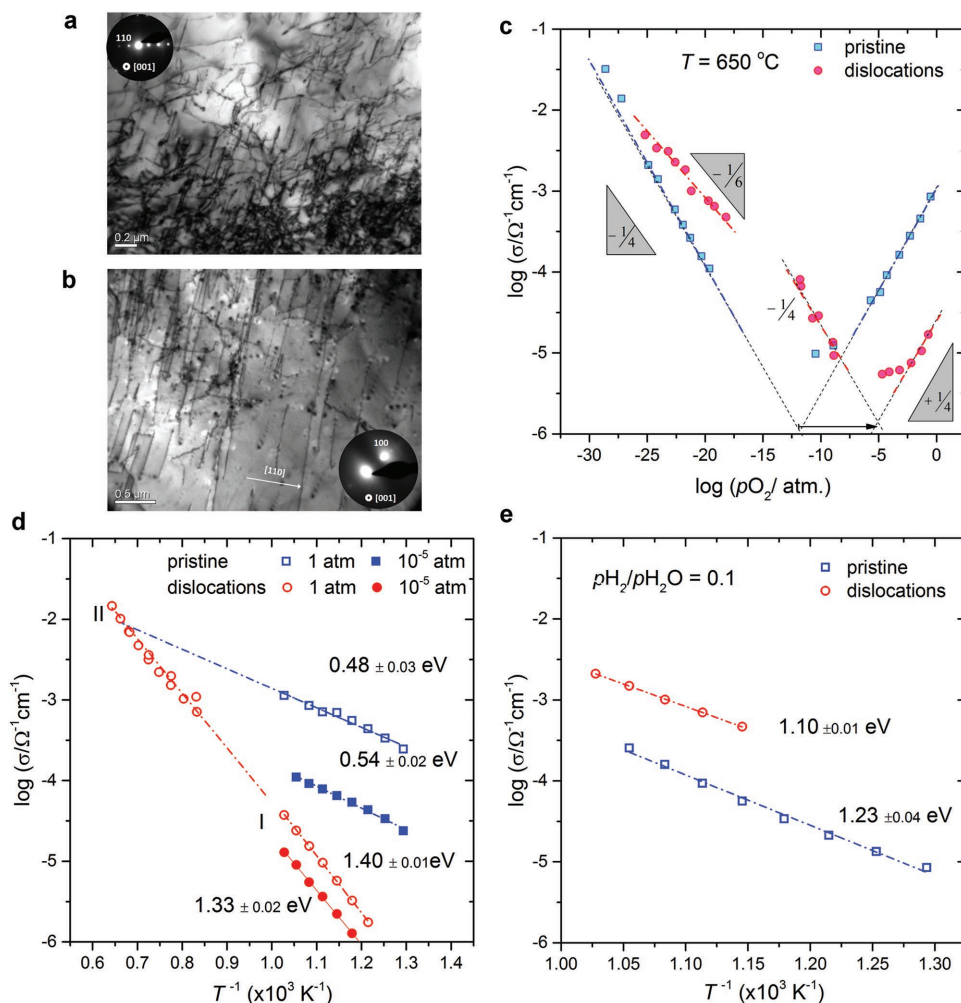


Figure 1. Effect of dislocations on SrTiO₃ defect chemistry. a,b) Bright field TEM image of compressed SrTiO₃ single crystal, specimens prepared from two different locations, with beam axis parallel to [001]. c) Electrical conductivity measured at 650 °C as a function of oxygen partial pressure, $p\text{O}_2$. d) Electrical conductivity as a function of temperature at two different high $p\text{O}_2$ conditions (1 atm and 10⁻⁵ atm). “I” and “II” represent two data sets from the low and high temperature measurements performed in two different setups. e) Electrical conductivity as a function of temperature at a low $p\text{O}_2$ with $p\text{H}_2/p\text{H}_2\text{O} = 0.1$. In panels (c)–(e), pristine represents the undeformed single crystal SrTiO₃, and dislocations represents the SrTiO₃ plastically deformed in hot uniaxial compression to form a high density of dislocations as shown in panels (a) and (b).

significantly higher $p\text{O}_2$ (Figure 1c) in the dislocations specimen is consistent with the reduction in hole concentration at the expense of increased electron concentration. This upshift in electron density is also consistent with the introduction of the regime at lower $p\text{O}_2$ that exhibits a $-1/6$ slope, in agreement with the predictions of Equation S5 (Supporting Information) for which the intrinsic reduction reaction is dominant. The same $-1/6$ slope behavior was also observed by Moos and

Hardtl^[53] and Choi and Tuller^[57] for single crystal bulk SrTiO₃, but at much higher temperature (>1000 °C) and lower $p\text{O}_2$ values (<10⁻¹⁵ bar). Under very low $p\text{O}_2$, a high concentration of electrons could lead to an inversion layer (i.e., the concentration of electrons exceeding the concentration of oxygen vacancies close to the dislocations), for example see Table 1 in ref. [58]. Such an inversion layer leads to a weaker $p\text{O}_2$ dependence of conductivity in space charge regions, for instance, when the

Table 1. Summary of activation energies and bandgap for the pristine and the dislocations SrTiO₃. ΔH_{red} : enthalpy of reduction; ΔH_{ox} : enthalpy of oxidation (oxygen incorporation); $E_{\text{a,e}^-}$: activation energy for electron conduction; $E_{\text{a,h}^+}$: activation energy for hole conduction; and E_{g} : bandgap energy calculated from enthalpy of oxidation and reduction, $E_{\text{g}} = (\Delta H_{\text{red}} + \Delta H_{\text{ox}})/2$.

Sample	$E_{\text{a,h}^+}$ [eV]	ΔH_{ox} [eV]	$E_{\text{a,e}^-}$ [eV]	ΔH_{red} [eV]	E_{g} [eV]
Pristine	0.48	0.96	1.23	5.62	3.29
Dislocations	1.40	2.80	1.10	4.58	3.49
Literature ^[51,53,57,60]	0.4–0.8	0.8–1.6	0.9–1.2	5.2–6.3	3.0–3.4

bulk conductivity shows $-1/4$ slope with pO_2 , the space charge region conductivity shows a weaker $-1/8$ slope. This could be a reason to observe a weak pO_2 dependence of electron conductivity (n-type, $-1/6$ slope in Figure 1c) in the dislocations specimen. A similar observation was also shown in the surface space charge dominated SrTiO₃ thin films.^[59] Alternatively, a transition from space charge controlled to the bulk situation is possible under decreased Debye length at very low pO_2 . In such case, the interpretation in terms of intrinsic electronic compensation (see Equations S3–S5 in the Supporting Information) can be assumed to be correct.

The temperature dependence of the electrical conductivities measured for both the pristine and the dislocations specimens at 1 and 10^{-5} atm, are reported in Figure 1d. The pristine specimen exhibited activation energies of 0.48 ± 0.03 and 0.54 ± 0.02 eV at 1 atm and 10^{-5} atm, respectively. The dislocations specimen exhibited considerably larger activation energies of 1.40 ± 0.01 and 1.33 ± 0.02 eV at 1 atm and 10^{-5} atm, respectively. To investigate whether the unusual electrical properties of the dislocations specimen were due to a nonequilibrated (frozen-in) point defect concentration and distribution, the conductivity measurements were also done at higher temperatures, up to 1280 °C in a high temperature setup (labeled as data set II in Figure 1d). No crossover to properties characteristic of the pristine SrTiO₃ specimen was observed, suggesting that the modified defect chemistry and electrical properties were not due to nonequilibrated (frozen) point defects, but rather to persistent dislocations influencing charge carrier density and transport. Temperature-dependent results measured under considerably more reducing conditions established by use of a hydrogen–water buffer mixture of $pH_2/pH_2O = 0.1$, are reported in Figure 1e. Under these reducing conditions, the pristine and dislocations specimens exhibited activation energies of 1.23 ± 0.04 and 1.10 ± 0.01 eV, respectively. In contrast to the higher pO_2 data reported in Figure 1d, here the dislocation specimen shows the higher conductivity, consistent with the behavior shown in Figure 1c, but with no significant change in activation energy.

The measured activation energies characterizing the electrical conductivity in the pristine and the dislocations SrTiO₃ specimens provide further insights into how the dislocations alter the defect formation and transport enthalpies. The reduction and oxidation enthalpies (Equations S2 and S10, respectively), as well as the calculated bandgap (Equation S14, Supporting Information) for both samples are summarized in Table 1. For the dislocations specimen, the electrical conductivity data and the calculated enthalpy values are only effective or mean values, given that the crystal is inhomogeneous because of the presence of dislocations (see, Figure 1a,b). The enthalpy of reduction was derived from Equation S4 (Supporting Information) for the dislocations specimen and from Equation S7 (Supporting Information) for the pristine sample at constant pH_2O/pH_2 instead of constant pO_2 by using the relations given in Equations S16 and S17 (Supporting Information). The enthalpies of oxidation and reduction and the bandgap values derived for the pristine specimen are in agreement with previous reports. For the dislocations specimen, however, we see a significant decrease in (apparent) reduction enthalpy and an increase in (apparent) oxidation enthalpy and bandgap energy. Typically, electrons follow

a $-1/6$ slope^[50,53,54] only at higher temperatures (>1000 °C) and very low pO_2 ($<10^{-15}$ atm) in bulk single crystal SrTiO₃. Recent theoretical calculations^[9,36,61] in SrTiO₃ and CeO₂ revealed that dislocation cores reduce the V_O formation energy. That prediction is consistent with our experimental observation here, and this is the likely reason for the appearance of the $-1/6$ slope and the shift to higher pO_2 for the conductivity minimum in the dislocations SrTiO₃ specimen. Finally, the much increased value of the activation energy for hole conduction for the dislocations SrTiO₃ of $E_{a,h} \approx 1.4$ eV. This value is similar to activation barriers characterized by transport in space charge zones as observed around grain boundaries in micro or nanocrystalline SrTiO₃.^[41,52,62,63] For the case of dislocations as studied here, the high activation energy of hole conduction is likewise attributed to space charge zones, as discussed below.

To confirm that the above-presented modified defect chemistry of SrTiO₃ is largely due to dislocations, we annihilated^[55] the dislocations by annealing the dislocations specimen at 1400 °C for 12 h in air. Based on the above analysis, annihilation of dislocations should give rise to the recovery of the SrTiO₃ bulk defect chemistry. Figure 2a, indeed confirms that the electrical properties of the annealed dislocations specimen (labeled as dislocations-anneal) is nearly identical to that of pristine SrTiO₃. Likewise, only minor changes in activation energy between these two samples at high as well as at low pO_2 , as shown in Figure 2b were observed. This confirms that the modified defect chemistry of the dislocations specimen is due to dislocations induced by plastic deformation.

The significant changes in the point defect equilibria revealed by electrical measurements above can be expected to have a strong impact on the oxide ion diffusion kinetics as well. Figure 3a shows the normalized ¹⁸O concentration measured by secondary ion mass spectroscopy (SIMS) as a function of penetration depth after ¹⁸O exchange and diffusion at 600 °C and 0.5 bar pO_2 for 24 h. These profiles reveal markedly lower isotope penetration depths, i.e., a significantly lower oxygen ion diffusion coefficient for the dislocations compared to the pristine SrTiO₃. This finding may seem counterintuitive due to the common belief that pipe diffusion of atoms along dislocations in metals are often found to be orders of magnitude greater than in dislocation-free specimens. As explained below, the key difference between the diffusion trends observed here compared to those in metals are the electrostatic interactions that exist between oxygen vacancies and charged dislocation cores in SrTiO₃ missing in metallic systems.

3. Discussion

In SrTiO₃, extended defects such as surfaces^[37,40,64,65] and grain boundaries^[41,63,65,66] are net positively charged due to preferential formation (low formation energy) of oxygen vacancies, V_O (in Kroeger–Vink notation^[67]). To maintain electroneutrality in the oxide overall, the excess positive charge at the extended defect core is electrostatically compensated by depletion of positively charged point defects and enrichment of negatively charged point defects, forming a space charge region adjacent to the defect core. This description is consistent with our recent atomistic computations^[36] that predicted oxygen vacancy

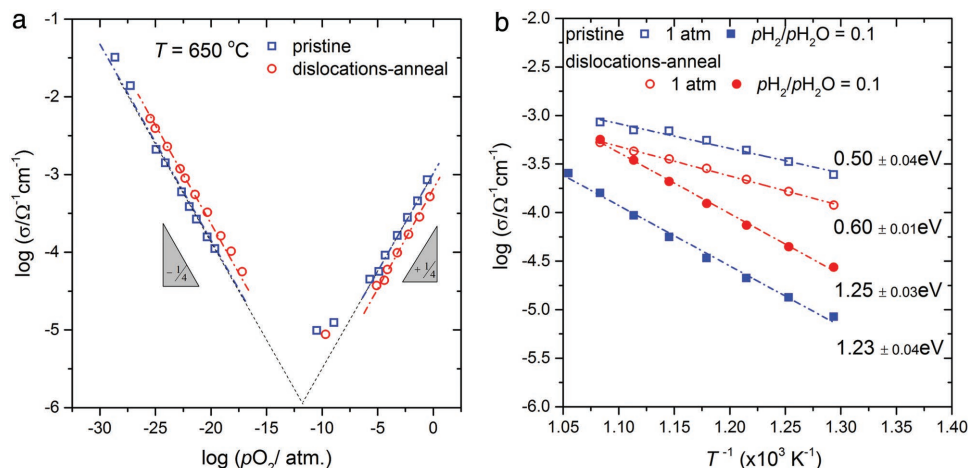


Figure 2. Annihilation of dislocations. a) Electrical conductivity as a function of oxygen partial pressure at 650 °C and b) as a function of reciprocal temperature with corresponding activation energies noted at high and low $p\text{O}_2$, for the pristine and the dislocations-anneal specimens. The dislocations-anneal corresponds to the state after annealing of the dislocations SrTiO₃ crystal at 1400 °C for 12 h in air.

enrichment at the dislocation core, and oxygen vacancy depletion within the space charge zone surrounding edge dislocations in SrTiO₃. The width of the space charge region, also known as the Mott–Schottky length (λ^*), depends on the electrostatic potential, dopant concentration, and temperature as previously described.^[52] Based on the Fe impurity concentration found in the SrTiO₃ studied in this work and typical space charge potentials on the order of 0.2–0.4 V at 600 °C, reported to exist at SrTiO₃ boundaries,^[52] the Mott–Schottky length in SrTiO₃ is calculated to be 70–100 nm. Dislocations that are closer than 200 nm (or dislocation density $>10^9\text{ cm}^{-2}$) apart should therefore have overlapping space charge regions. TEM images of our dislocations specimen (Figure 1b) show dislocations separated by 50–200 nm (and several dislocation networks with less than 50 nm spacing). Thus, in this sample, the space charge zones can be expected to overlap, leaving no bulk region within the sample unaffected (as shown numerically below in Figure 3). It is worth noting that this behavior is very similar to the mesoscopic situation of nanocrystalline SrTiO₃.^[63]

Going back to Figure 3a, we see evidence for the ¹⁸O diffusion profiles of both the pristine and the dislocations SrTiO₃ being influenced by space charge effects. This becomes evident for the pristine specimen, but only just adjacent to the surface. Surface space charge layers are known to slow oxygen ion diffusion in SrTiO₃ due to V_{O}^{\bullet} depletion just beneath the surface.^[37,64,65] This is reflected by the two distinct slopes^[64,65] evident in the ¹⁸O profile for the pristine specimen shown in Figure 3a—a slower oxide ion diffusion regime with a small isotope penetration depth near the surface within the space charge region, labeled regime-I, and the deeper fast oxide ion diffusion regime due to bulk diffusion, labeled regime-II. Interestingly, the dislocations SrTiO₃ specimen show only a regime-I. This behavior demonstrates that the dislocations SrTiO₃ consists of overlapping space charge regions, thereby eliminating the bulk component of the diffusion profile in Figure 3a. To quantitatively analyze the ¹⁸O diffusion profiles under the effect of space charge regions, we have simulated the isotope profiles using COMSOL Multiphysics. The model considers a dislocation grid with 50 nm periodicity. Since this distance is shorter

than twice the Mott–Schottky length in SrTiO₃ (140–200 nm), this model mimics the space charge overlap situation (see the Experimental Section and Section S3 (Supporting Information) for model details and the simulation procedure). The simulated diffusion profiles are in agreement with the experimental data, as seen in Figure 3a. The simulated 2D spatial profiles of the space charge potential (ϕ), oxygen vacancy concentration ($[V_{\text{O}}^{\bullet}]$), and oxygen tracer diffusion (D_{O}^*) along the isotope penetration depth (plane vertical to the surface) in the pristine and dislocations specimens are shown in Figure 3b–d and a brief summary of quantitative results are shown in Table S1 in the Supporting Information. As expected, these profiles are highly heterogeneous within the bulk of the dislocations SrTiO₃. Also, importantly, the profiles in Figure 3b–d confirm the space charge regions around the dislocations overlap within the dislocations specimen, completely changing the bulk behavior of SrTiO₃.

Given that the electrostatic potential distribution does not reach 0 V anywhere within the bulk of the dislocations SrTiO₃ (Figure 3b), this in turn leads to a significant depletion in oxygen vacancy concentration (and therefore, D_{O}^*) everywhere within the dislocations SrTiO₃. The value for D_{O}^* (shown in Figure 3d) derived here for pristine SrTiO₃ (bulk diffusion) is $3 \times 10^{-18}\text{ m}^2\text{ s}^{-1}$, comparable to D_{O}^* values reported in the literature^[68–70] for SrTiO₃ single crystals with oxygen diffusivities characterized by higher oxygen vacancy migration energies, i.e., 0.9–1 eV. Impurity–vacancy association (especially with Fe impurities, as the case in our samples)^[40,71,72] are known to lead to higher effective migration enthalpies. D_{O}^* in the dislocations SrTiO₃ varies exponentially with distance between the dislocations, i.e., $3 \times 10^{-22}\text{ m}^2\text{ s}^{-1}$ in very close vicinity of the dislocations and $3 \times 10^{-19}\text{ m}^2\text{ s}^{-1}$ between the dislocations (see Figure 3d). The experimental ¹⁸O profiles (Figure 3a) arise from an area-averaging across the xy planes sputtered during depth profiling, with no lateral spatial resolution. Therefore, we average the simulated D_{O}^* in a similar fashion over the xy plane for the dislocations SrTiO₃ (see Figure S3 in the Supporting Information), providing a simpler comparison with the pristine specimen. These area-averaged profiles are also those shown

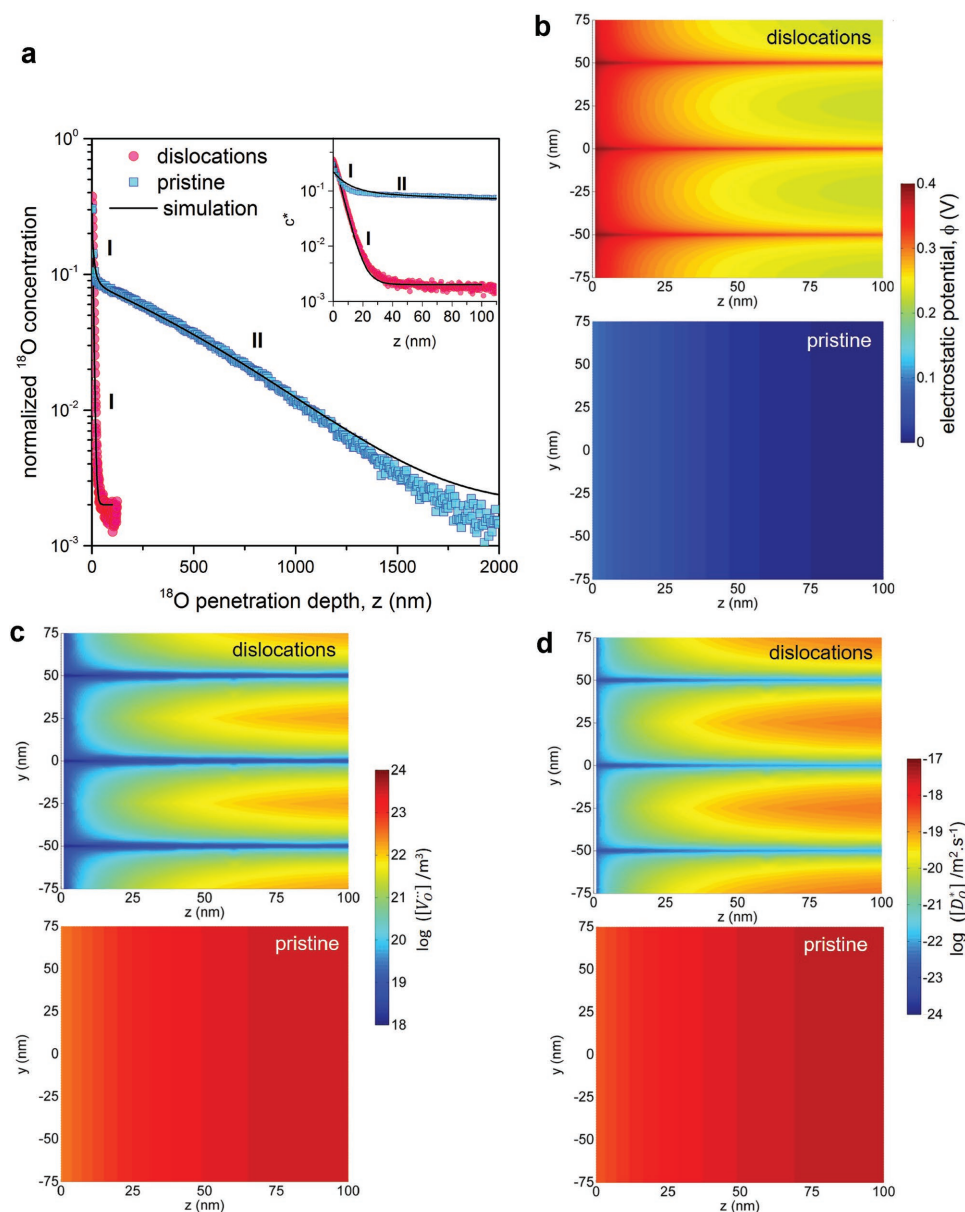


Figure 3. Effect of dislocation space charge regions on the oxygen diffusion in SrTiO₃. a) Experimental ¹⁸O isotope depth profiles for the pristine (solid squares) and dislocations (solid circles) SrTiO₃ after ¹⁸O exchange at 600 °C and 0.5 bar *p*O₂ for 24 h. The inset shows the initial steep drop in ¹⁸O concentration (regime-I) due to surface space charge regions followed by the bulk diffusion (regime-II). Dislocations SrTiO₃ exhibits only regime-I, indicating overlapped space charge regions without any unaffected bulk medium. The simulated isotope profile (solid lines) is obtained by solving the Poisson–Boltzmann equation combined with the time-dependent diffusion equation, resulting in a space charge potential at the dislocation core, $\phi_{\text{dis}}^0 = 0.34$ V, and a surface exchange coefficient, $k_s^* = 1.5 \times 10^{-11}$ cm s⁻¹. The 3D model for the dislocations SrTiO₃ specimen consists of a periodic arrangement of dislocations at 50 nm spacing extending from the surface (at *z* = 0 nm) into the bulk. Computed distribution of the b) electrostatic potential (ϕ), c) oxygen vacancy concentration (V_{O}), and d) oxygen tracer diffusion coefficient (D_{O}^*) on the *yz* plane (perpendicular to the surface) in the pristine and dislocations SrTiO₃.

as the simulated data in Figure 3a. The area-averaged D_{O}^* is approximately three orders of magnitude lower (3×10^{-21} m² s⁻¹ at a penetration depth of ≈ 25 nm) in the dislocations SrTiO₃ compared to that in the pristine specimen (3×10^{-18} m² s⁻¹) at 600 °C. In this analysis, we have ignored the contribution of the dislocation cores to diffusion. Recently, we^[36] and others^[37,38] have shown by atomistic simulations that dislocation cores (with ≈ 1 nm cross sections) provide either no acceleration or

only a few times higher D_{O}^* than the bulk of SrTiO₃. Given their very small volume (≈ 1 nm diameter) and higher migration barrier for oxygen vacancies, the effect of dislocation cores on oxygen diffusion is negligible compared to the large decrease of oxygen vacancy concentration within the much wider space charge regions. This is also consistent with there being no net pipe diffusion of oxygen along dislocations in SrTiO₃, as discussed above. Although the oxygen diffusion experiments were

performed at the high pO_2 regime, we believe pipe diffusion will not be an outcome even under a strongly reducing atmosphere ($pO_2 < 10^{-15}$ bar). The core charge should remain positive (with a weak dependence on pO_2 ^[73]) because it is a result of a strong structural driving force and any variation due to redox reactions (by varying pO_2) is comparatively small. The weak pO_2 dependence of the core charge means a comparable oxygen vacancy concentration exists at the core both at low and at high pO_2 , but the mobility remains low as we reported earlier. At the same time, the increase of vacancy concentration in the bulk with reducing pO_2 is expected to be more significant than at the core. The presence of a positively charged core would continue to result in a space charge zone depleted in oxygen vacancies, effectively reducing the oxygen diffusion coefficient, including the low pO_2 regime.

We note that it is possible to obtain similar diffusion profiles when simulating the case of a higher surface potential (see Figure S5 in the Supporting Information) even in the absence of dislocations that penetrate into the specimen. However, this interpretation does not explain the reasons for the (hole) conductivity drop at high pO_2 (Figure 1c). Based on the high temperature compression of single crystals, TEM analysis, and electrical conductivity measurements; a consistent picture close to the experimental results is only obtained by simulating overlapping space charge regions by closely spaced dislocations extending in to the bulk (Figure 3b).

The space charge model and analysis presented in this study offer a self consistent analytical picture capable of describing our independently obtained electrical conductivity and ¹⁸O diffusion measurements. The reduction in oxygen ion diffusivity and in p-type conductivity, both dependent on the concentration of positively charged species (oxygen vacancies (Figure 3c,d) and holes (Figure 1c,d), respectively), and the increase in n-type conductivity dependent on negatively charged species (i.e., electrons (Figure 1c,e)) are well explained by the space charge regions formed in response to the positively charged dislocations in SrTiO₃.

As a result, the changes in the electronic charge carrier density decreased the p-type conductivity by approximately a factor of 50, increased the n-type conductivity (for data following the $-1/4$ slope) by the same factor of 50, and shifted the extrapolated conductivity minimum to higher pO_2 by seven orders of magnitude (Figure 1c, see Supporting Information section S.7 for additional sidenotes on the conductivity flattening at intermediate pO_2). Based on Equation S2 (Supporting Information), it is clear that an increase in electron concentration by a factor of 10 should result in a decrease in oxygen vacancy concentration by a factor of 100. Based on the measured decrease in oxygen diffusion, the doubly positive charged $V_O^{\bullet\bullet}$ concentration averaged over x - y plane (Figure S3, Supporting Information) was reduced by approximately three orders of magnitude upon the introduction of dislocations (Figure 3c). Slow mobility of oxide ions along dislocation cores, combined with the significantly reduced concentration of oxygen vacancies within the extended space charge zones, slows down oxygen diffusion within SrTiO₃, and the space charge zone is the dominant factor due to its larger volume fraction than the dislocation core. The reduction in the $V_O^{\bullet\bullet}$ concentration is close to the expected decrease by 3.6 orders (p-type conductivity decreased by 1.8

orders magnitude at 600 °C, Figure 1d) of magnitude based on Equation S2 (Supporting Information). Hence, utilizing the electrical data to derive the effective space charge potential gave a consistent result with that obtained from the diffusion profile (see Figure S6 in Section S7 in the Supporting Information).

4. Conclusions

In summary, these findings have profound implications for the properties of functional oxides. Together with recent results^[32,33] on TiO₂, our results demonstrate that the introduction of 1D extended defects can markedly modify the defect, electrical, and transport properties of functional oxides, without changing their nominal chemical composition. Indeed, these two studies show the critical importance of the dislocation core polarity on the defect and transport properties. While the negative dislocation core charge in TiO₂ resulted in marked enhancements in ionic conductivity due to positively charged titanium interstitials as well as more modest increases in p-type conductivity,^[32–34] on the contrary, the positive dislocation core charge in SrTiO₃, as determined in this study resulted in quite the opposite effect, leading to markedly reduced ionic conductivity due to positively charged oxygen vacancies and more modest reductions in p-type conductivity. Furthermore, while the dislocation cores themselves are locally confined to the sub-nanometer dimensions, the excess charge at the core results in electrostatic effects that can extend tens to hundreds of nanometers, thereby altering the properties of a large fraction of the bulk of the material. Control of dislocation density in thin oxide films (as described in the Introduction) can pave the way for a new approach for tuning of functional oxides. This approach can be viewed as plastic strain engineering for altering the macroscopic properties of oxides, akin to the recent developments in elastic strain engineering,^[6,7] and alternative to the existing chemical doping methods. Plastic strain engineering in oxides that form extended space charge regions has the potential for significantly affecting the point-defect-dependent functionalities in electrochemical and/or electronic applications such as thin film oxide electronics, memristive systems, sensors, and microsolid oxide fuel cells.

5. Experimental Section

Dislocations Generation and Characterization: Dislocations were created by a hot uniaxial compression (field assisted hot press) of nominally undoped SrTiO₃ single crystal substrates along [001] ($5 \times 5 \times 1$ mm³, MTI, California and Crystec GMBH Germany) contained in a graphite mold with SiC spacers under inert atmosphere. Soft graphite sheets were used to avoid friction between spacers and the crystal, as well as to obtain uniform stress across the crystal surface. One set of samples was prepared from the crystals compressed at Max Planck Institute, Stuttgart at 1400 °C and 40 MPa for 5 min., and these samples were used for the TEM and SIMS experiments. One set of samples was prepared at Harvard University, USA, at a slightly lower temperature, i.e., at 1200 °C (due to experimental limitations with the hot press), and at 40 MPa for 5 min. This sample was used for electrical characterization. The elastic modulus of SrTiO₃ varies with temperature only to a small extent with temperature relevant to hot compression; previous studies (both experimental^[74] as well as computational^[75]) showed $\approx 7\%$ variation in the elastic modulus with 200 °C variation in temperature. Therefore, the

two samples used, respectively, for TEM and SIMS, and for electrical measurements are expected to have comparable dislocation densities, even though a different distribution cannot be excluded. All samples, including pristine samples, were equilibrated in air at 1200 °C for 5 h prior to compression as well as after to reoxidize and re-equilibrate the point defects. The samples were characterized with a Philips CM 200 TEM with a point-to-point resolution of 2.7 Å for viewing dislocations.

Electrical Characterization: The defect chemistry of SrTiO₃ is investigated by measuring its electrical properties as a function of oxygen partial pressure (*p*O₂) and temperature. The specimens were electroded by applying Pt paste as current collecting electrodes. A wide range of *p*O₂ was achieved by mixing O₂/Ar, CO/CO₂, and H₂/H₂O in appropriate ratios. A home-built zirconia based *p*O₂ sensor was placed close to the sample to measure the *p*O₂. A Solartron 1260 impedance analyzer was used for collecting impedance data between frequencies 1 MHz to 100 mHz. The sample resistance and capacitance data were obtained by fitting the impedance data to an equivalent circuit with the aid of ZView software from Scribner Associates Inc.

Oxygen Isotope Experiments: Oxygen isotope (¹⁸O) exchange was performed for both samples in a quartz chamber. The samples were subjected to preannealing in 0.5 bar oxygen (¹⁶O) atmosphere at 600 °C for 240 h prior to ¹⁸O anneal for 24 h, according to Fielitz and Borchardt^[76]. The samples were heated and quenched rapidly between ¹⁶O/¹⁸O exchanges by a movable furnace to minimize transient diffusion during cooling/heating. To obtain similar thermal history, samples were annealed at 1000 °C for 5 h prior to isotope exchange. The crystal surface is not chemically treated, as it is known that surface reconstruction (or preferential termination) strongly influences the surface dislocation density as well as oxygen incorporation kinetics. The isotope depth profiles were analyzed by time of flight secondary ion mass spectroscopy (ToF-SIMS, IONTOF GmbH, Germany).

Numerical Simulations: Numerical simulations of the isotope profiles from tracer diffusion experiments were performed with COMSOL Multiphysics software. The Poisson–Boltzmann equation, combined with the time-dependent diffusion equation was solved as described in the literature,^[38,64] to obtain the spatially dependent profiles of the electrostatic potential, the oxygen vacancy concentration, and the oxygen tracer diffusion in the space charge and the bulk regions of the specimen. To mimic the experimental conditions of the space charge overlap in the specimen with dislocations, the dislocation space charge zones with radial geometry around dislocation cores have been modeled with 50 and 100 nm grid periodicity (see Figure S4 in Section 5 in the Supporting Information for results of the 100 nm periodicity) at the surface (*xy* plane) and in the bulk (*z* direction). The pristine specimen is simplified to a 1D model which is homogeneous on the *xy* plane with only a surface space charge potential. More details of the model are provided in Section S3 in the the Supporting Information.

Supporting Information

Supporting Information is available from the Wiley Online Library or from the author.

Acknowledgements

The authors thank M. Kelsch (electron microscopy facility, P. van Aken) and T. Acarturk (interface analysis facility, U. Starke) at the Max Planck Institute for Solid State Research, Stuttgart, Germany for helping with transmission electron microscopy and SIMS measurements, respectively. K.K.A. and J.M. also thank Dr. Rotraut Merkle (Max Planck Institute for Solid State Research, Stuttgart, Germany) for discussions. Authors thank Prof. David Clarke for providing the hot press facilities and Dr. Samuel Shian for helping with compression experiments at Harvard University, Cambridge, MA, USA. B.Y. thanks Prof. Rainer Waser for useful discussions on the joint effect of cores and space charges of

dislocations on the effective diffusion coefficients along dislocations in SrTiO₃. This work was partially supported by NSAF through the Massachusetts Institute of Technology Materials Research Science and Engineering Center DMR-1419807. The defect modeling was supported by DOE-Basic Energy Sciences, Grant No. DE-SC0002633. Computational work was supported by the Consortium for Advanced Simulation of Light Water Reactors (CASL), an Energy Innovation Hub for Modeling and Simulation of Nuclear Reactors under U.S. Department of Energy Contract No. DE-AC05-00OR22725.

Keywords

dislocations, electrical properties, mixed ionic electronic conductor, oxide ion diffusion, point defects

Received: January 15, 2017

Revised: February 16, 2017

Published online:

- [1] A. Ohtomo, H. Y. Hwang, *Nature* **2004**, 427, 423.
- [2] N. Sata, K. Eberman, K. Eberl, J. Maier, *Nature* **2000**, 408, 946.
- [3] M. Sillassen, P. Eklund, N. Pryds, E. Johnson, U. Helmersson, J. Böttiger, *Adv. Funct. Mater.* **2010**, 20, 2071.
- [4] C.-P. Chang, M.-W. Chu, H. T. T. Jeng, S.-L. Cheng, J. G. G. Lin, J.-R. Yang, C. H. H. Chen, *Nat. Commun.* **2014**, 5, 3522.
- [5] S. Lee, W. Zhang, F. Khatkhatay, Q. Jia, H. Wang, J. L. MacManus-Driscoll, *Adv. Funct. Mater.* **2015**, 25, 4328.
- [6] J. Li, Z. Shan, E. Ma, *MRS Bull.* **2014**, 39, 108.
- [7] B. Yildiz, *MRS Bull.* **2014**, 39, 147.
- [8] A. Kushima, B. Yildiz, *J. Mater. Chem.* **2010**, 20, 4809.
- [9] T. X. T. Sayle, M. Cantoni, U. M. Bhatta, S. C. Parker, S. R. Hall, G. Möbus, M. Molinari, D. Reid, S. Seal, D. C. Sayle, *Chem. Mater.* **2012**, 24, 1811.
- [10] M. Kubicek, Z. Cai, W. Ma, B. Yildiz, H. Hutter, J. Fleig, *ACS Nano* **2013**, 7, 3276.
- [11] S. Schweiger, M. Kubicek, F. Messerschmitt, C. Murer, J. L. M. Rupp, *ACS Nano* **2014**, 8, 5032.
- [12] N. Tsvetkov, Q. Lu, Y. Chen, B. Yildiz, *ACS Nano* **2015**, 9, 1613.
- [13] F. C. Frank, J. H. van der Merwe, *Proc. R. Soc. A* **1949**, 198, 216.
- [14] J. W. Matthews, A. E. Blakeslee, *J. Cryst. Growth* **1974**, 27, 118.
- [15] S. C. Jain, A. H. Harker, R. A. Cowley, *Philos. Mag. A* **1997**, 75, 1461.
- [16] F. Sandiumenge, N. Bagués, J. Santiso, M. Paradinas, A. Pomar, Z. Konstantinovic, C. Ocal, L. Balcells, M.-J. Casanove, B. Martínez, *Adv. Mater. Interfaces* **2016**, 3, 1600106.
- [17] C. Korte, A. Peters, J. Janek, D. Hesse, N. Zakharov, *Phys. Chem. Chem. Phys.* **2008**, 10, 4623.
- [18] S. Azad, O. A. Marina, C. M. Wang, L. Saraf, V. Shutthanandan, D. E. McCready, A. El-Azab, J. E. Jaffe, M. H. Engelhard, C. H. F. Peden, S. Thevuthasan, *Appl. Phys. Lett.* **2005**, 86, 131906.
- [19] I. Kosacki, C. M. Rouleau, P. F. Becher, J. Bentley, D. H. Lowndes, *Electrochem. Solid-State Lett.* **2004**, 7, A459.
- [20] G. I. Taylor, *Proc. R. Soc. A* **1934**, 145, 362.
- [21] W. T. Read, *Philos. Mag.* **1954**, 45, 775.
- [22] K. P. McKenna, *J. Am. Chem. Soc.* **2013**, 135, 18859.
- [23] R. Konta, T. Ishii, H. Kato, A. Kudo, *J. Phys. Chem. B* **2004**, 108, 8992.
- [24] K. Szot, W. Speier, R. Carius, U. Zastrow, W. Beyer, *Phys. Rev. Lett.* **2002**, 88, 75508.
- [25] K. Szot, W. Speier, G. Bihlmayer, R. Waser, *Nat. Mater.* **2006**, 5, 312.
- [26] C. Lenser, Z. Connell, A. Kovács, R. Dunin-Borkowski, A. Köhl, R. Waser, R. Dittmann, *Appl. Phys. Lett.* **2013**, 102, 183504.
- [27] C. Lenser, A. Koehl, I. Slipukhina, H. Du, M. Patt, V. Feyer, C. M. Schneider, M. Lezaic, R. Waser, R. Dittmann, *Adv. Funct. Mater.* **2015**, 25, 6360.

- [28] F. Messerschmitt, M. Kubicek, S. Schweiger, J. L. M. Rupp, F. Messerschmitt, M. Kubicek, S. Schweiger, J. L. M. Rupp, *Adv. Funct. Mater.* **2014**, *24*, 7448.
- [29] E. Mikheev, B. D. Hoskins, D. B. Strukov, S. Stemmer, *Nat. Commun.* **2014**, *5*, 3990.
- [30] S. I. Cha, K. H. Hwang, Y. H. Kim, M. J. Yun, S. H. Seo, Y. J. Shin, J. H. Moon, D. Y. Lee, *Nanoscale* **2013**, *5*, 753.
- [31] K. Domen, A. Kudo, T. Onishi, *J. Catal.* **1986**, *102*, 92.
- [32] K. K. Adepalli, M. Kelsch, R. Merkle, J. Maier, *Adv. Funct. Mater.* **2013**, *23*, 1798.
- [33] K. K. Adepalli, M. Kelsch, R. Merkle, J. Maier, *Phys. Chem. Chem. Phys.* **2014**, *16*, 4942.
- [34] K. K. Adepalli, *Ph.D. Thesis*, University of Stuttgart **2013**.
- [35] D. Kajewski, R. Wrzalik, M. Wojtyniak, M. Pilch, J. Szade, K. Szot, C. Lenser, R. Dittmann, R. Waser, *Phase Transitions* **2011**, *84*, 483.
- [36] D. Marrocchelli, L. Sun, B. Yildiz, *J. Am. Chem. Soc.* **2015**, *137*, 4735.
- [37] V. Metlenko, A. H. H. Ramadan, F. Gunkel, H. Du, H. Schraknepper, S. Hoffmann-Eifert, R. Dittmann, R. Waser, R. A. De Souza, *Nanoscale* **2014**, *6*, 12864.
- [38] S. P. Waldow, R. A. De Souza, *ACS Appl. Mater. Interfaces* **2016**, *8*, 12246.
- [39] I. Denk, J. Claus, J. Maier, *J. Electrochem. Soc.* **1997**, *144*, 3526.
- [40] R. A. De Souza, V. Metlenko, D. Park, T. E. Weirich, *Phys. Rev. B* **2012**, *85*, 174109.
- [41] R. Hagenbeck, R. Waser, *J. Appl. Phys.* **1998**, *83*, 2083.
- [42] R. Di Capua, M. Radovic, G. M. De Luca, I. Maggio-Aprile, F. Miletto Granozio, N. C. Plumb, Z. Ristic, U. Scotti di Uccio, R. Vaglio, M. Salluzzo, *Phys. Rev. B* **2012**, *86*, 155425.
- [43] Y. Hu, O. K. Tan, J. S. Pan, X. Yao, *J. Phys. Chem. B* **2004**, *108*, 11214.
- [44] W. Jung, H. L. Tuller, *J. Electrochem. Soc.* **2008**, *155*, B1194.
- [45] D. P. Fagg, V. V. Kharton, A. V. Kovalevsky, A. P. Viskup, E. N. Naumovich, J. R. Frade, *J. Eur. Ceram. Soc.* **2001**, *21*, 1831.
- [46] S. Burnside, J. E. Moser, K. Brooks, M. Gra, D. Cahen, M. Gratzel, *J. Phys. Chem. B* **1999**, *103*, 9328.
- [47] F. Lenzmann, J. Krueger, S. Burnside, K. Brooks, M. Grätzel, D. Gal, S. Rühle, D. Cahen, *J. Phys. Chem. B* **2001**, *105*, 6347.
- [48] T. Menke, P. Meuffels, R. Dittmann, K. Szot, R. Waser, *J. Appl. Phys.* **2009**, *105*, 66104.
- [49] R. Muenstermann, T. Menke, R. Dittmann, R. Waser, *Adv. Mater.* **2010**, *22*, 4819.
- [50] N. H.-H. Chan, R. K. Sharma, D. M. Smyth, *J. Electrochem. Soc.* **1981**, *128*, 1762.
- [51] R. Waser, *J. Am. Ceram. Soc.* **1991**, *74*, 1934.
- [52] I. Denk, J. Claus, J. Maier, *J. Electrochem. Soc.* **1997**, *144*, 3526.
- [53] R. Moos, K. H. Hardtl, *J. Am. Ceram. Soc.* **1997**, *80*, 2549.
- [54] C. Ohly, S. Hoffmann-Eifert, X. Guo, J. Schubert, R. Waser, *J. Am. Ceram. Soc.* **2006**, *89*, 2845.
- [55] Z. Wang, S. Karato, K. Fujino, *Phys. Earth Planet. Inter.* **1993**, *79*, 299.
- [56] W. Sigle, C. Sarbu, D. Brunner, M. Rühle, *Philos. Mag.* **2006**, *86*, 4809.
- [57] G. Choi, H. Tuller, *J. Am. Ceram. Soc.* **1988**, *71*, 201.
- [58] S. Kim, J. Fleig, J. Maier, *Phys. Chem. Chem. Phys.* **2003**, *5*, 2268.
- [59] R. A. De Souza, F. Gunkel, S. Hoffmann-Eifert, R. Dittmann, *Phys. Rev. B* **2014**, *89*, 241401.
- [60] G. M. Choi, H. L. Tuller, D. Goldschmidt, *Phys. Rev. B* **1986**, *34*, 6972.
- [61] L. Sun, D. Marrocchelli, B. Yildiz, *Nat. Commun.* **2015**, *6*, 6294.
- [62] P. Balaya, J. Jamnik, J. Fleig, J. Maier, *J. Electrochem. Soc.* **2007**, *154*, P69.
- [63] P. Lupetin, G. Gregori, J. Maier, *Angew. Chem. Int. Ed.* **2010**, *49*, 10123.
- [64] R. A. De Souza, M. Martin, *Phys. Chem. Chem. Phys.* **2008**, *10*, 2356.
- [65] R. A. De Souza, *Adv. Funct. Mater.* **2015**, *25*, 6326.
- [66] R. A. De Souza, *Phys. Chem. Chem. Phys.* **2009**, *11*, 9939.
- [67] F. A. Kroger, H. J. Vink, *Solid State Phys. Adv. Res. Appl.* **1956**, *3*, 307.
- [68] I. Denk, F. Noll, J. Maier, *J. Am. Ceram. Soc.* **2005**, *80*, 279.
- [69] A. Yamaji, *J. Am. Ceram. Soc.* **1975**, *58*, 152.
- [70] A. E. E. Paladino, L. G. G. Rubin, J. S. S. Waugh, *J. Phys. Chem. Solids* **1965**, *26*, 391.
- [71] K. A. Müller, *J. Phys.* **1981**, *42*, 551.
- [72] M. Schie, R. Waser, R. A. De Souza, *J. Phys. Chem. C* **2014**, *118*, 15185.
- [73] Z. Zhang, W. Sigle, R. A. De Souza, W. Kurtz, J. Maier, M. Rühle, *Acta Mater.* **2005**, *53*, 5007.
- [74] E. A. Patterson, M. Major, W. Donner, K. Durst, K. G. Webber, J. Rödel, *J. Am. Ceram. Soc.* **2016**, *99*, 3411.
- [75] A. Boudali, M. D. Khodja, B. Amrani, D. Bourbie, K. Amara, A. Abada, *Phys. Lett. A* **2009**, *373*, 879.
- [76] P. Fielitz, G. Borhardt, *Solid State Ionics* **2001**, *144*, 71.